Green Synthesis of TiO_2 Nanoparticles and Study of Impedance Spectroscopy of TiO_2-Polypyrrole Nanocomposites

Kousik Dutta
Assistant Professor in Physics
Department of Physics, Behala College, Parnashree; Kolkata- 700060; INDIA
Author for correspondence: duttakousik2003@yahoo.co.in

Received May 23, 2015 Accepted June 4, 2015

ABSTRACT Nanotechnology is a new star in the science horizon with many valuable applications and promises to offer. It includes the synthesis and utilization of nanostructure materials ranging from 1 to 100 nm. Mostly these materials are generally (or "could be") produced via the laborious and hazard-prone physical and chemical methods but the green synthesis approaches easier, safe and scalable have been recently developed. Among other metal oxides nanoparticles, Titanium oxide (TiO_2) nanoparticles have been mostly exploited for their photocatalytic, antimicrobial and antiparasitic applications. Titanium dioxide nanoparticles (TiO_2-NPs) were synthesized using the aqueous leaf extract of Aloe barbadensis as a reducing and fabricating agent.. Based on the HRTEM and FESEM analysis, X-ray diffraction (XRD), the biosynthesized NPs were found to be polydispersed and predominantly spherical in shape, with an average size of ~20 nm. Complex impedance and dielectric permittivity of TiO_2-PPY nanocomposite have been investigated as a function of frequency and temperature at different compositions. The dielectric permittivity 2500 is observed. Large value of permittivity is well described by Maxwell-Wagner polarization. Broad and asymmetric dielectric spectra are analyzed by Harviliak - Nigami relaxation function.

Key words **:** Green Synthesis, TiO_2 nanoparticles, TiO_2-PPY nanocomposites, dielectric properties.

INTRODUCTION:

Nanotechnology is emerging as a rapidly growing field with its application in science and technology for the purpose of manufacturing new materials at the nanoscale level [1]. Nanotechnology has gained massive applications in the fields of biology and pharmacology [2]. Such materials can be designed to exhibit novel and significantly improved physical, chemical and biological properties, phenomena and processes as a result of the limited size of their constituent particles or molecules, and enabling their usage in a wide range of innovative applications [3-5]. To avoid the use of toxic organic solvents and severe reaction conditions (temperature, pressure, and long refluxing time) for the preparation of nanomaterials, researchers recently have been exploring the possibilities of preparing nanomaterials in aqueous medium with the help of stabilizing or capping agents [6]. Generally metal nanoparticles can be

prepared and stabilized by physical, chemical and biological methods with little modifications for different metals, [7-11]. The properties of nanoparticles and its applications are different and dependent on their size, distribution and morphology, [12] or even on synthesis methods.

Increasing sensibility towards green chemistry and biological processes has led to develop an environment-friendly process for the synthesis of non-toxic nanoparticles. A vast array of biological resources available in nature including living plants, [13], plant products, plant crud extracts, algae, fungi, yeast, [14], bacteria,[15] and viruses could all be employed for synthesis of nanoparticles. Biological methods are regarded as safe, cost-effective, biocompatible, non-toxic sustainable and environment friendly processes, In addition, most bioprocesses occur under normal air pressure and temperature, resulting in vast energy savings, high-yield and low cost, [16].

Titanium dioxide (TiO_2) is a naturally abundant metal oxide which occurs in three different forms anatase, brookite and rutile phases [17]. TiO_2 NPs are white colored n-type semi-conductor having high thermal stability, excellent optical and dielectrical properties, bio-compatibility and non-toxicity [18-19]. Due to these properties TiO_2 NPs are used in vast applications such as photo catalyst, lithium ion batteries, optoelectronic devices, reduction of H_2O_2, solar cells [20-21], etc. Like wise it is also used in sunscreens, pigments, paints, antimicrobial coatings owed to its high refractive index against sunlight [22]. Different types of approaches are available for synthesis of titanium dioxide nano particles, those are Sol-Gel [23], Hydrothermal [24], Solvothemal [25], Microwave Assisted [26], co-precipitation [27], Chemical Vapour Deposition. [28]

The usage of plant parts for synthesis of nanoparticle can be advantageous owing to the cost-effective, eco-friendly, not required of high energy, toxic chemicals, pressure and temperature [29]. Last few years many researchers prepared TiO_2 nanoparticles using bio synthesis method. Ecliptaprostrata leaf extract and Titanium hydroxide solution were used for preparing TiO_2 nanoparticles [30]. Bio- mediated TiO_2 nanoparticles were synthesized by using Potassium exafluorotitanate and bacterium of Bacillus subtilis [31]. Titanium (IV) isopropoxide and Rice straw used for bio synthesis of TiO_2 nanoparticles [32]. Rutile phase TiO_2 nanoparticles

were synthesized from the Annona squamosa peel extract and $TiO(OH)_2$ [33]. The present work is based on the *Aloe vera* plant extract. *Aloe Vera* is oldest medicinal plant ever known. The *Aloe Vera* extract contains water soluble substances like Aloe emodin, Chrysophonal, and Helminthospor. These compounds act as reducing agents to produce TiO_2 particles from the precursor [34-35].

Polypyrrole (PPY) is one of the most studied conducting polymers because of its good electrical conductivity, environmental stability and relatively easy synthesis [36-37]. Monomers are polymerized in the aqueous solution in the presence of metal and oxide nanoparticles to obtain nanocomposites. The composites of different kinds of inorganic oxides such as NiO, SnO_2, CuO, ZnO, CeO_2, etc [38-39] have been synthesized by various chemical routes. Colloidal dispersion of inorganic nanoparticles within the polymer matrix, as suggested by Han and Armes, is a very efficient and novel chemical process to prepare homogeneous Composites [40].

TABLE I: Weight percentage of pyrrole (x), activation energy from grain boundary (E_{gb}), grain conductivity (E_g), activation energy E_τ) real part of relative dielectric permittivity (ϵ_1) at room temperature (RT)

Sample	x	E*gb* (meV)	E*g* (meV)	E_τ (meV)	ϵ1(RT)
S1	20	98	57	58	2500
S2	35	84	49	50	2200
S3	50	76	38	39	2100
S4	65	68	31	30	1700

The Synthesis part of the present paper is mainly divided in two parts. In the 1st part TiO_2 nanoparticles were synthesize using aloe Vera leaf extract. After synthesize these nanoparticles are embeded in the conducting PPY to prepare TiO_2-PPY nanocomposite In the Observation the study of impedance spectroscopy of various TiO_2-PPY nanocomposites samples as a function of frequency and temperature.

MATERIALS AND METHODS

All the chemicals were of analytical grade and purchased from Merck (India) and used without further purification. Pyrrole (AR grade) was purified and stored at -15^{0}C in a refrigerator prior to use. APS oxidant was used as received and de-ionized water was employed for preparing all the solutions and reagents. The samples were characterized by x-ray powder diffraction patterns employing a scanning rate of 0.02 0 per 2 sec in 2θ range from 10 to 90 using a Philips (PW1710) x-ray diffractometer equipped with monochromatized Cukα radiations. The nanocrystalline powder was pressed inside the sample holder and X-ray data were collected in step scan mode.

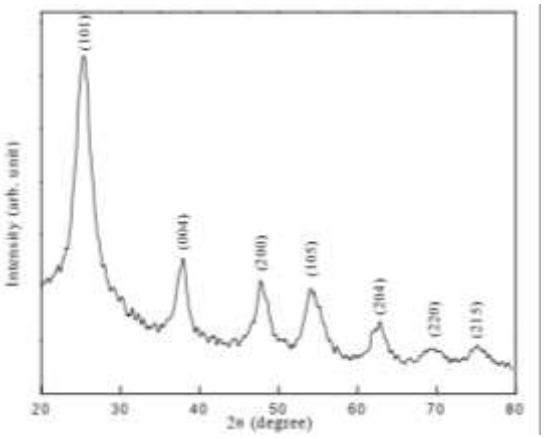

Figure 1: X-ray diffraction pattern of PPY-TiO2 nanocomposite sample S1.

Morphological studies were performed with JEOL JSM6700F Scanning electron microscope (SEM). Transmission electron micrograph (TEM) was taken from JEOL, JEM 2010 with acceleration voltage of 200 KV. The temperature dependent capacitance (C) and dielectric loss factor (D) were measured by Agilent 4192 Impedance Analyzer. The electrical contacts were made by silver paint on both sides of the sample. Dry powdered sample were made into pellets using a steel die of 1 cm diameter in a hydraulic press under a pressure of 5 ton. The thickness of the samples varies from 0.07 cm to 0.11 cm. For electrical measurements the electrical contacts were made by silver paint.

A. Preparation of aloe Vera leaf extract

Fresh and healthy *Aloe Vera* plant was collected locally. One of the selected leaves was cut and washed twice with tap water followed by distilled water to remove dust particles and other contaminants. 60g of the leaves was weighed using electronic weighing balance and transferred into a 600 ml beaker containing 250 ml distilled water. The contents were boiled for 2h at 80°C. The extract was filtered using Whatman filter paper. The filtrate was stored for the synthesis of nanoparticles.

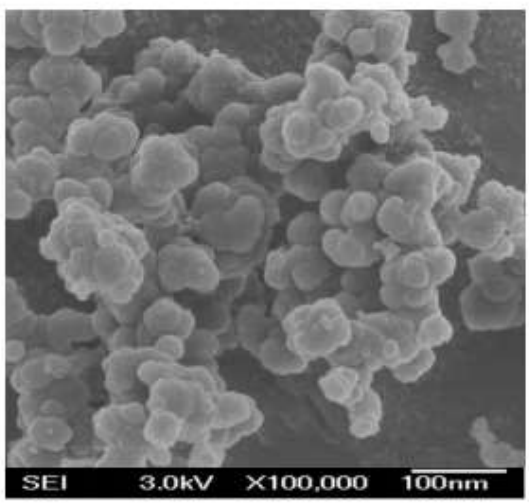

Figure 2: Scanning electron micrograph of sample S1.

B. Synthesis of Titanium Oxide (TiO_2) nanoparticles by aloe Vera leaf extract:

To synthesis the TiO_2 nanoparticles, dissolve 1.0 N of Titanium Chloride ($TiCl_4$) in 100 ml of Millipore water. Added leaves extract drop wise under constant stirring up to achieve pH of solution became 7.

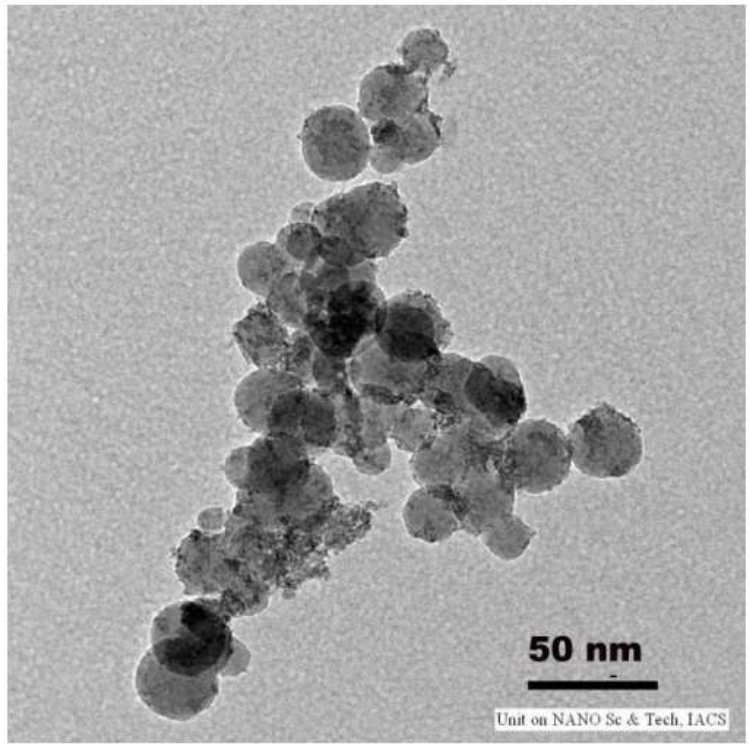

Figure 3: Tunneling electron micrograph of sample S1.

The mixture was subjected to stirring for 4 hours continuously. The NPs formed during the process were collected by centrifugation (10,000 rpm) and repeatedly washed with ethanol (absolute). to remove the by-products. The nanoparticles were dried at 100°Cfor overnight and calcined at 500°Cfor 4 hours.

C. Synthesis of TiO_2 - PPY nanocomposite:

The required quantity of TiO_2 nanoparticle was ultrasonically dispersed in 50 ml deionized water. Pyrrole monomer of known volume was slowly added into the dispersion under sonication at room temperature. Then the aqueous solution of APS maintaining a pyrrole : APS mole ratio of 1:1.25 was added drop wise into the previous solution. After few hours the resulting solution was turned into black color which indicates the formation of polypyrrole. The solution was then kept under sonication for about 8 hours to ensure complete polymerization. Finally, the resulting black dispersion were centrifuged. The resulting nanocomposites were washed thoroughly with distilled water for several times. Different compositions of nanocomposite samples by varying the weight percentage of pyrrole(polypyrrole) were prepared as shown in Table I.

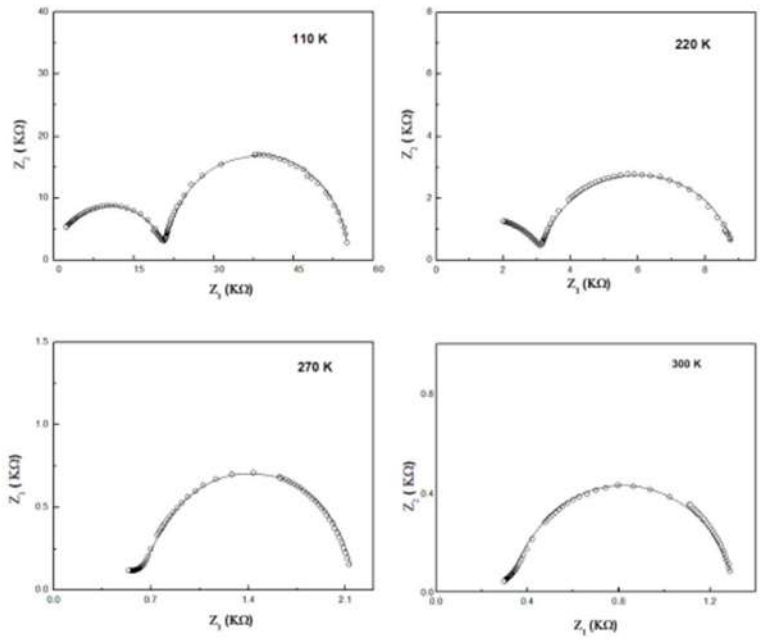

Figure 4: Impedance spectra of the sample S1 at four different temperatures. The solid lines are fits to the proposed equivalent circuit for the sample.

RESULTS AND DISCUSSION:

Fig. 1 shows the characteristic peaks of X-ray diffraction (XRD) of the sample S1. The spectra reveals the presence of anatase phase of Titania in the nanocomposites. The crystallite size of the TiO2 nanoparticles in the composite sample S1 is calculated following the Scherrer's relation (using 101 face) **[41]**

$$D = K\lambda/\beta\cos\theta \qquad \textbf{(1)}$$

where K=0.89, D represents crystallite size (nm), λ, the wavelength of *CuKα* radiation and β, the corrected value at half width of the diffraction peak. At 2θ=25.36^o (101), which is the characteristics peak of TiO2, is chosen to calculate the average diameter and it comes out to be 25 nm, which is consistent with that obtained from TEM studies.

The scanning electron micrograph (SEM) of the nanocomposite sample S1 is shown in Figure 2. The TiO_2 nanoparticles are well dispersed and are of spherical in shape with uniform diameter lying in the range from 25- 30 nm. Larger particle size may be due to the aggregation of smaller particles in the presence of polymer matrix.

Figure 3. shows the TEM micrograph of the TiO_2 - polypyrrole nanocomposite S1 sample. In this micrograph nearly, spherical crystallites are observed. The mean particle size of pure TiO_2 is in the range of 20-25 nm. Larger particle size due to the aggregation of smaller particles in the presence of polymer matrix. The nano particles are polydispersed

and are of spherical shape with uniform diameter lying in the range from 15-25 nm. After the formation of the composites the particles are found to be entrapped into polypyrrole chains. Immediate conclusion is that the colloid particles are not simply mixed up or blended with the polymer, they are rather encapsulated by the polypyrrole chains.

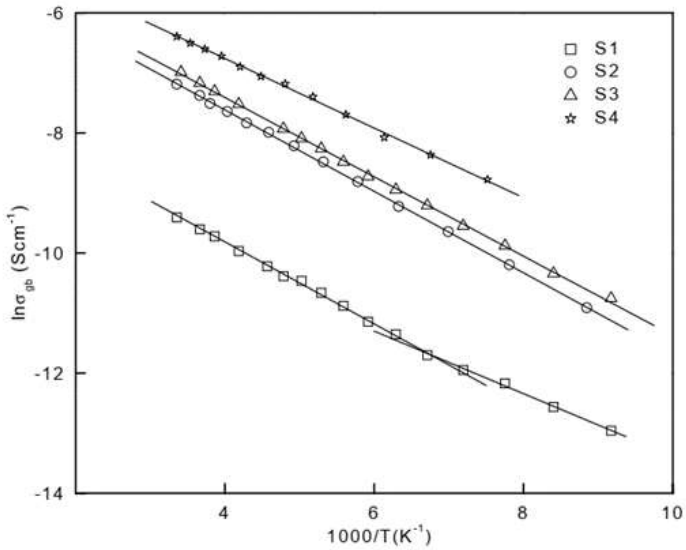

Figure 5: Impedance spectra of the sample S1 at four different temperatures. The solid lines are fits to the proposed equivalent circuit for the sample.

Figure 4. represents the complex impedance, $Z=Z_1 +iZ_2$ plots for the sample S1 at different temperatures. At low temperature, two incomplete semicircles are observed. The high frequency contribution dominates with lowering of temperature. The features of the impedance spectra of polycrystalline composite materials primarily depend on the microstructure. The SEM micrographs indicate that the nanocomposites consist of nanometer size grains which introduce more grain boundaries within the samples. The impedance spectra can be interpreted by the equivalent circuit consisting of series connected parallel resistance (R) and capacitance (C) components as shown in Figure 5. The position of the maximum arc in the impedance diagram is determined by the relation $\omega_{max}RC = 1= 1$, where $\omega_{max}RC = 1$, where $\omega_{max} = 2\pi f$, f is the applied frequency. The larger values of R and C at grain boundary lead to smaller ω_{max} compared to grain. Moreover, ω_{max} lies outside the available frequency range and only some portions of semicircles are obtained at higher temperature. The grain and grain boundary responses are analyzed by the following relations

$$Z_1 = \frac{R_g}{1+(\omega R_g C_g)^2} + \frac{R_{gb}}{1+(\omega R_{gb} C_{gb})^2}$$

$$Z_2 = R_g\left[\frac{\omega R_g C_g}{1+(\omega R_g C_g)^2}\right] + R_{gb}\left[\frac{\omega R_{gb} C_{gb}}{1+(\omega R_{gb} C_{gb})^2}\right] \quad \text{(2) \& (3)}$$

where (R_g, R_{gb}) and (C_g, C_{gb}) are resistance and capacitance of grain and grain boundary respectively. Equations (2) and (3) represent two ideal semicircles whose centers lie on the real Z_1 axis. The constant phase elements (CPE) capacitors $C(\omega) = B(i\omega)^{n-1}$ are assumed to analyze the more flattened semicircles. The parameter B is constant for a given set of experimental data. The exponent n varies between 0 and 1. The impedance of CPE behaves as an ideal capacitor for n = 1 and ideal resistor for n = 0. The solid lines in Figure 4 represent the best fitted calculated values. Both C_{gb} and C_g are weak temperature dependent.

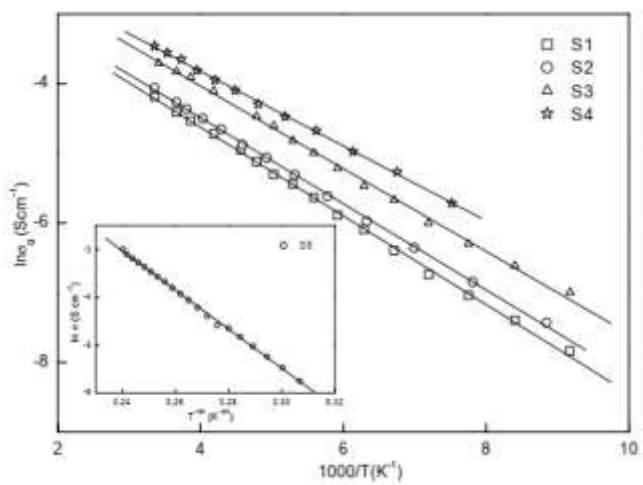

Figure 6: Impedance spectra of the sample S1 at four different temperatures. The solid lines are fits to the proposed equivalent circuit for the sample. Inset represents the impedance data of polypyrrole matrix.

Grain (σ_g) and grain boundary (σ_{gb}) conductivities have been calculated from the best fitted values of R_g and R_{gb}. Figures 5 and 6 show the temperature dependence of grain and grain boundary conductivity. The estimated grain boundary conductivity is about 100 times lower than that of grain conductivity. The grain boundary (E*gb*) and grain (E*g*) activation energies are presented in Table I. Both σ_g and σ_{gb} follow Arrhenius type process with temperature as evidence from the plots in Figures 5 and 6. The activation energy of the grain interior is smaller than that of grain boundary. The conductivity of grain boundary region is mainly determined by the microstructure. The temperature dependence of conductivity of PPY obeys Mott's three dimensional variable range hopping process. [42-43] Thermally activated conductivity variation

suggests that PPY is not dominating the conduction process.

The value of Ɛ1 decreases with decrease of TiO_2 content. At high frequency greater than 1 MHz, $Ɛ_1$ reaches to about 2500. Figures 7 represents the temperature dependence of $Ɛ_1$ for S1. The step like transition to lower values shifts to lower frequency with decreasing temperature. The high frequency value of Ɛ1 is almost independent of temperature. The unusually large dielectric constant can be explained by interfacial Maxwell-Wagner (MW) interfacial relaxation commonly applied in heterogenous system. The nanocomposites consist of conducting grains and resistive grain boundaries. Under the application of external electric field, the charge carriers can easily migrate the grains but are accumulated at the grain boundaries. This process can produce large polarisation and high dielectric constant. The small conductivity of grain boundary contributes to high value of dielectric constant at low frequency. The static dielectric constant based on the equivalent circuit in Figures 4 can be expressed as

$$\epsilon_1(0) = \frac{R_g^2 C_g + R_{gb}^2 C_{gb}}{C_0 (R_g + R_{gb})^2} \quad (4)$$

Resistance and capacitance of grain boundary are much larger than that of grain. In MW polarisation, dielectric constant under such condition can be approximated from eq.(4) as $Ɛ1(0) = C_{gb}/C_0$. A large value of C_{gb} leads to very high value of dielectric constant. The ratio of TiO_2 and PPY modifies the microstructure i.e. grain boundary capacitance. This may be the possible reason for different values of Ɛ1 for different compositions.

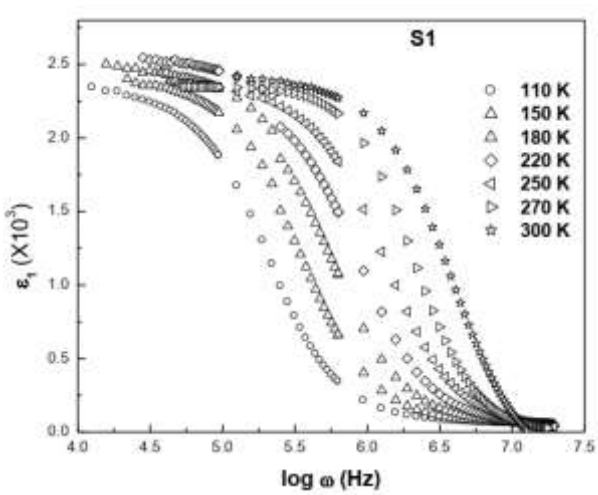

Figure 7: Frequency dependence of the real part of relative dielectric constant ($Ɛ_1$) at different temperatures for the sample S1.

The dielectric loss spectra ε_2 as a function of frequency for S1 are shown in Figures 8 for different temperatures. Two relaxation peaks in the measured frequency domain are appeared at room temperature. The positions of the peaks move to lower frequency with the decrease of temperature. The dielectric response has been analyzed by the most generalized Havriliak-Negami (HN) function [44].

$$\epsilon^* = \sum_{\delta}[\epsilon_\infty + \frac{\epsilon_s - \epsilon_\infty}{(1+(i\omega\tau)^\beta)^\alpha}]\delta \quad (5)$$

where tau is the average relaxation time which is given at the frequency of maximum dielectric loss. The difference $\Delta\varepsilon = \varepsilon_s - \varepsilon_\infty$ is known as the dielectric relaxation strength. The parameter β describes the distribution of the relaxation time of the system. Debye relaxation is obtained for α = 1 and β = 1. The parameters α and **β** ranging between 0 and 1 are symmetric and asymmetric broadening of dielectric spectra. The solid lines in Figures 8 show that the experimental data are reasonably good fitted with the calculated value of HN function.

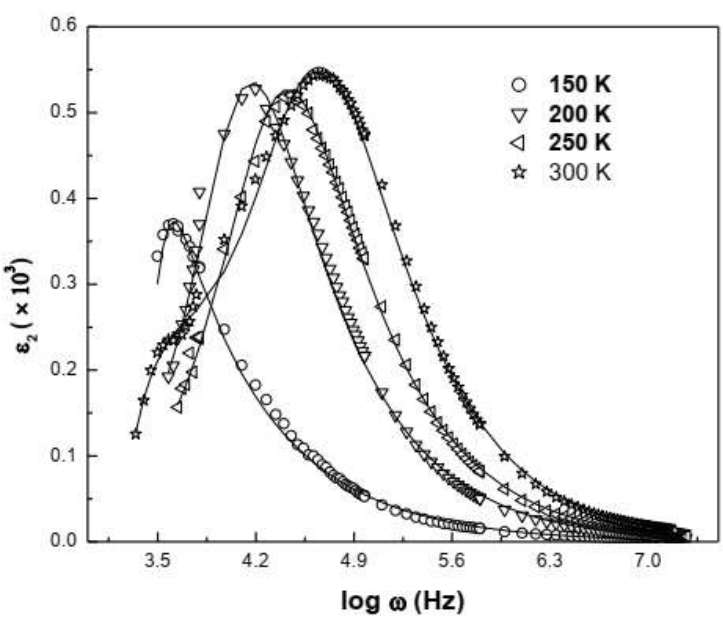

Figure 8: Frequency dependence of imaginary component of dielectric constant ε_2 at selected temperatures for the sample S1. The solid lines are fits to Eq. 5.

The value of **β** is different from unity which implies non- Debye relaxation process. This parameter manifests that the dielectric dispersion has a broad distribution of

relaxation time. The dielectric strength Δε increases with increase of temperature. The relaxation times, τ at different temperatures are obtained from the best fitted data to eqn. (6).

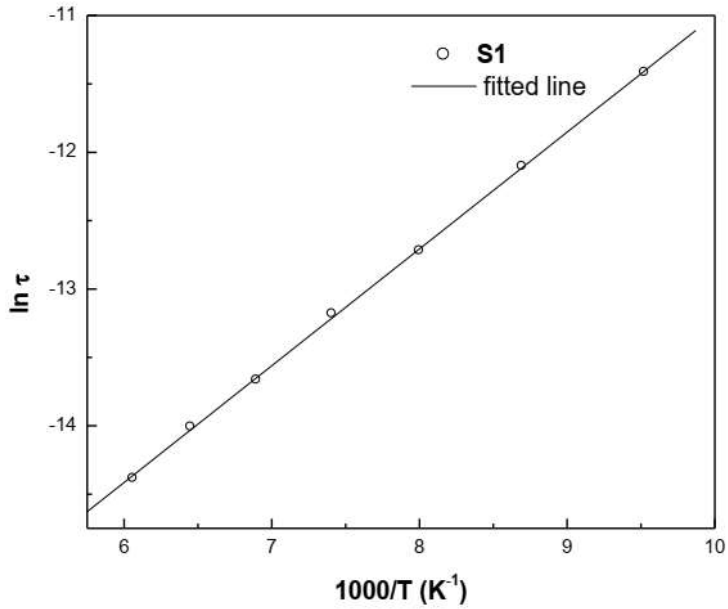

Figure 9: Arrhenius plot of dielectric relaxation time vs frequency at different temperatures for the sample S1

The linear behavior of the Arrehenius plot of ln τ against 1/T suggest that the temperature variation of τ can be described by thermally activated Arrhenius law,

$$\tau = \tau_0 exp(E_\tau / kT) \quad (6)$$

where τ_0 is the relaxation time at high temperature, E_τ is the activation energy of dielectric process and k is Boltzmann constant. The slope of the best fitted straight line gives the activation energy as shown in Table I. The most interesting fact is that the activation energies are in excellent agreement with the values obtained from grain conductivity.

CONCLUSION:

Impedance data demonstrate the existence of electrically semiconducting grains and more resistive grain boundaries. The values of dielectric constant exhibit large variations with compositions, temperature and frequency. The dielectric response at the lower frequency is characterized by Maxwell-Wagner relaxation. The variations of microstructure with compositions render different dielectric constants.

REFERENCES:

[1] Abdelrahim SI, Almagboul A.Z., Omer M.E. and Elegami A, 2002 Antimicrobial activity of Psidium guajava L. Fitoterapia 73 713-715

[2] Wang Y, Wang J, Wu M, Deng X, Wen T and Chen C, et al., 2010, J Nanosci Nanotechnol 10(11) 7121-7125.

[3] Kelsall R W, Hamley I W and Geoghegan. M. 2005 Nanoscale Science and Technology. John Wiley & Sons Ltd, 473p.

[4] Salata O. 2004 J Nanobiotechnol 2 3-6

[5] Gwinn MR, Vallyathan V. 2006 Nanoparticles: Health effects-pros and Cons. Environ Health Perspect 114 1818-1825.

[6] Shervani Z, Yamamoto Y, 2011 Mat Lett 65 92-95

[7] Zhou R., Wu X., Hao X., Zhou F., Li H, Li H. and W. Rao. 2008, Nuclear Instruments and Methods in Physics Research B: Beam Interactions with Materials and Atoms, 266(4) 599-603

[8] Soomro R.A, Hussain S. T, Sherazi Sirajuddin, Memon1 N, Shah M. R, Kalwar N.H , Hallam K. R. and Shah A. 2014 Adv. Mat. Lett. 5(4) 191-198

[9] Salam HA. Rajiv P. Kamaraj M, Jagadeeswaran P. Gunalan S. and Sivaraj R. 2012, I. Res. J. Biological Sci, 1(5) 85-90

[10] Sarkar M.B. Datta J. Mondal D. and Mukhopadhyay S. 2013 International Journal of Research in Engineering and Technology 2(8) 400-404

[11] Khashan K.S 2013 Eng. & Tech. Journal 31(1) 39-48

[12] Pérez J, Bax, L and Escolano C. 2005 Roadmap report on nanoparticles. Barcelona, Spain: Willems & van den Wildenberg (W&W) (ES/NL). pp. 57.

[13] Bali R, Razak N, Lumb A. and Harris A.T 2006 The synthesis of metallic nanoparticles inside live plants. Laboratory for Sustainable Technology, School of Chemical and Biomolecular Engineering, The University of Sydney, NSW, Australia. 4p.

[14] Castro L, Blázquez M.L Muñoz J.Á González F.G and Ballester, A 2014 Reviews in Advanced Sciences and Engineering 3 1-18.

[15] Jha Z., Behar N., Sharma S N., Chandel G., Sharma D. and Pandey M. 2011 Nano Vision, 1(2) 88-100.

[16] Makarov VV. Love, A J. Sinitsyna OV Makarova SS. Yaminsky IV. Taliansky ME, Kalinina NO. 2014 Acta. Naturae, 6(1) 35-44

[17] Mohan Rajneesh, Drbohlavova Jana and Hubalek Jaromir, 2013 Nanoscale Research Letters. 8(1) 4

[18] Fox M.A, Dulay M.T, 1993, Chem. Rev. 93 341–357

[19] Varahalarao Vadlapudi, 2014 173 I J P A C. 9 167

[20] Gomathi Devi L, Kottam Nagaraju, Narasimha Murthy B., Girish Kumar S., 2010 Journal of Molecular Catalysis A. 328 44–52

[21] Raghu Reddy C., Rao R.N and Prakash1 T.L, 2012 Archives of Applied Science Research. 4 (3) 1528-1531

[22] Shaw T, Simpson B , Wilson B, Oostman H., Rainey D, 2010 Dermatitis Storrs F21(4) 185–98.

[23] Thangavelu Kavitha, Annamalai Rajendran and Arulnandhi Durairajan, 2013 International Journal of Emerging Technology and Advanced Engineering, 3(1), 636.

[24] Shivaraju H.P, Byrappa. K., Vijaykumar T. M.S. and Ranganathaiah. C, ydrothermal 2010, Bulletin of the Catalysis Society of India 9 37

[25] Cao-Thang Dinh, Thanh-Dinh Nguyen, Freddy Kleitz and Trong-On Do, 2012. The Canadian Journal Of Chemical Engineering, 90, 8

[26] Lee Hanbin, Choi Minsik, Kye Younhee, Myoungyoung An, and Ik Mo Lee, 2012, Bull. Korean Chem. Soc, 33(5), 1969.

[27] Kamran Rasool, Muhammad Usman, Mushtaq Ahmad, Zahid Imran, M. A. Rafiq and M. M. Hasan, 2011 IEEE, 4-8.

[28] Wu Jie, Bai GuoRen, Jeffrey A. Eastman, Zhou Guangwen and Vijay K. 2005 Materials Research Society, 879E, Z7.12.1.

[29] G. Rajakumar, A.A. Rahuman, C. Jayaseelan, T. Santhoshkumar, S. Marimuthu, C. Kamaraj, A. Bagavan, A.A. Zahir, A.V. Kirthi, G. Elango, P. Arora, R. Karthikeyan, S. Manikandan, S. Jose, 2014 Parasitol. Res. 113 (2) 469–479.

[30]Rajakumar G., Rahuman, A.A. Priyamvada B., Khanna V.G., Kumar D.K., Eclipta P.J. Sujin, 2012 Mater. Lett. 68 115–117.

[31] Dhandapani P, Maruthamuthu S., Rajagopal G., 2012 J. Photochem. Photobiol. B: Biol. 11043–49.

[32] Ramimoghadam D, S. Bagheri, S.B. Abd Hamid 2014 BioMed Res. Int. 1–7

[33] Roopan S. M., Bharathi A., Prabhakarn A., Rahuman A. Abdul, Velayutham K., Rajakumar G., Padmaja R.D., Lekshmi M., Madhumitha G., 2012 Spectrochim. Acta Part A 98 86–90

[34] Kavanagh, F., "Analytical Microbiology. F. Kavanagh (ED)", VOL II, Academic Press New York, and London, P: 11, 1972.

[35] Zhang LL, Jiang YH, Ding YL, Povey M and York D. 2007 J.Nanopart. Res 9:479–489

[36] Torillo G, Garnier F, 1999 J. Electroanal. Chem. 135 172

[37] Skothim T. A. Elenbaumer R., Reynolds J. R. 1998 Handbook of conducting polymers, Marcel Dekker, New York,

[38] S. Maeda, S. P. Armes, 1995, Synt. Synt. Metals 73, 151

[39] Huang C. L., Matijevi E., 1995 J. Mater. Res. 10, 1327

[40] M. G. Han and S. P. Armes, 2003, J. Colloid and Interface Sci., 262, 418

[41] H. P. Klug and L. E. Alexander, X-ray diffraction procedures for polycrystalline and amorphous materials, John Wiley and Sons, New York, 1954, p491.

[42] N. F. Mott, E. Davis, Electronic Process in Non Crystalline Materials, 2nd ed., Oxford, Clarendon, 1979

[43] T. Skotheim and R. Elsenbaumer, 1998 Handbook of Conducting Polymers, Marcel Dekker, New York

[44] S. Havriliak and S. Negami, 1967 Polymer 8, 161